RSC Advances

This is an *Accepted Manuscript*, which has been through the Royal Society of Chemistry peer review process and has been accepted for publication.

Accepted Manuscripts are published online shortly after acceptance, before technical editing, formatting and proof reading. Using this free service, authors can make their results available to the community, in citable form, before we publish the edited article. This *Accepted Manuscript* will be replaced by the edited, formatted and paginated article as soon as this is available.

You can find more information about *Accepted Manuscripts* in the Information for Authors.

Please note that technical editing may introduce minor changes to the text and/or graphics, which may alter content. The journal's standard Terms & Conditions and the Ethical guidelines still apply. In no event shall the Royal Society of Chemistry be held responsible for any errors or omissions in this *Accepted Manuscript* or any consequences arising from the use of any information it contains.

ROYAL SOCIETY OF CHEMISTRY

www.rsc.org/advances

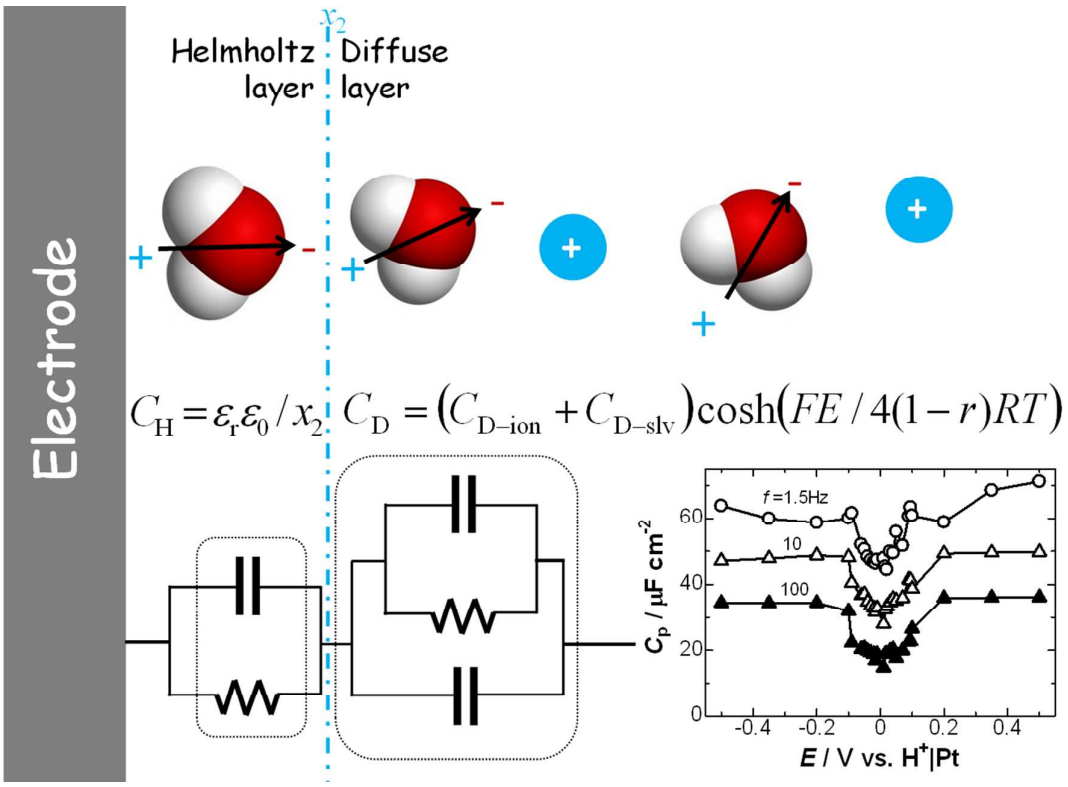

Equivalent circuit of double layer capacitance composed of the inner layer capacitance and the two components of diffuse layer capacitance with considering frequency-dependence.

RSC Advances Accepted Manuscript

Examination of the Gouy-Chapman theory for double layer capacitance in deionized latex suspensions

Xiaoyu Zhao, Koichi Jeremiah Aoki, Jingyuan Chen*, Toyohiko Nishiumi

Department of Applied Physics, University of Fukui, Bunkyo 3-9-1, Fukui 910-0017 Japan

Abstract

Electric double layer capacitance at platinum electrodes is controlled by dipole moments of solvent in the diffuse layer rather than that by ionic distribution, being different from at mercury electrodes. The controlling step is found by comparing capacitance vs. electrode potential curves in ionic solutions with those in deionized latex suspensions. The curves do not involve a valley shape of Gouy-Chapman (GC)-Stern's type until ionic concentrations are less than 0.05 mM, because measured capacitance is controlled by the inner layer. The valley shape at the low concentrations can be measured in deionized sulfonic latex suspensions, whose conductance is brought about by the ionic latex particles rather than the dissociated hydrogen ion. The expression for the capacitance by the ionic latex suspension is derived, which is demonstrated to be the same form of the potential dependence as for mono-valence ions. The ac-impedance data are obtained at parallel polycrystalline platinum wires without insulating shield. The valley shape is found, which is analyzed by the inverse plot of the capacitance against the hyperbolic cosine of the dimensionless applied potential. The linearity of the plots seems to support the GC-theory, but the capacitance values are much larger than those calculated from the GC-theory. The extra amount can be

* Corresponding author: e-mail jchen@u-fukui.ac.jp, fax +81 776 27 8753

RSC Advances Accepted Manuscript

attributed quantitatively to the orientation of solvent molecules by combining Debye's theory with the GC-theory.

key words: latex suspensions of polystyrene sulfonic acid; electric double layer capacitance; Gouy-Chapman-Stern model; Helmholtz layer

1. Introduction

Electric capacitance is an important measure of properties of electric double layers. The observed capacitance, C_d, is composed of the Helmholtz layer capacitance, C_H, and the diffuse layer capacitance, C_D [1-3], in a series connection:

$$1/C_d = 1/C_H + 1/C_D \quad (1)$$

because each layer is geometrically laminar [3]. The Helmholtz (inner) layer capacitance is given by

$$C_H = \varepsilon_r \varepsilon_0 / x_2 \quad (2)$$

where ε_r is the dielectric constant of solvent and x_2 is the distance of the closest approach of ions to the electrode. The inner layer capacitance has been assumed to be independent of electrode potential. It has been theoretically discussed by considering the orientation of solvent molecules in the solvation sheath on electrodes [4-7] and the clusters of solvent molecules with a dipole moments [8-10]. In contrast, the potential dependence of C_D for mono-valence electrolyte has been given by the Gouy-Chapman (GC) theory in the form [11,12]:

$$C_D = (2\varepsilon_r \varepsilon_0 F^2 c / RT)^{1/2} \cosh(F\phi / 2RT) \quad (3)$$

where c is the monovalent ionic concentration, ϕ is the dc-potential, R is the gas constant, F is the Faraday constant and T is temperature. Eq. (3) is valid only for low concentrations of ions, because the Poisson-Boltzmann distribution might overlap

RSC Advances Accepted Manuscript

theoretically ions in the double layer beyond their finite size. Several modifications of the GC theory includes finite size of ions [13-18], saturation of dielectric constants of solvents [19-22], numerical solutions [23,24] and computer simulation complicated by ionic properties [25,26], and electrode-size effects [27-30]. The recent advance of the behavior of the double layer has been reviewed by Kornyshev [15], especially in the light of the double layer of ionic liquids.

The potential variation of the GC theory allows us to separate C_H or C_D from the observed capacitance. A possible technique is to plot of $1/C$ against $1/\cosh(F\phi/2RT)$ to yield a line with an intercept, $1/C_H$, according to the combination of Eq. (1) and (3). The GC-term at $\phi = 0$ is $(2\varepsilon_0\varepsilon_r F^2 c/RT)^{1/2}$, of which numerical values are 7.2, 2.3, and 0.7 μF cm^{-2} for c = 1, 0.1 and 0.01 mM of aqueous solutions. In contrast, values of C_H (Eq. (2)) range from 1.0 to 1.7 μF cm^{-2} for x_2 (0.3 - 0.5 nm) at $\varepsilon_r = 6$ for the saturated dielectric constant of water [31]. Values of $1/C_D$ are smaller than those of $1/C_H$ at conventionally used concentrations of electrolyte so that C_D cannot be extracted by the plot. In order to determine C_D-component, it is necessary to use concentrations at least less than 0.01 mM. Such low concentration yields 1 MΩ resistance in the 1×1×1 cm^3 cube of the solution, which blocks accurate measurements of impedance. Indeed, an attempt of the accurate determination has not yet been reported, to our knowledge.

A strategy of overcoming the difficulty of the determination is to use suspensions of ion-incorporated microspheres, called ionic latex particles. Counterions are partially dissociated from the salt incorporated on the latex particles and are distributed near the particles even after the suspensions are deionized sufficiently [32-35]. For example, acidified polystyrene-sulfonate latex (PSS) suspensions dissociate hydrogen ion from the $-SO_3H$ moiety in salt solutions as a strong acid. When it is deionized, only 1% of hydrogen ions are dissociated, as has been observed by voltammetry [36]. The conductance of latex suspensions is brought about mainly with the Brownian motion of the multi-anion latex particles rather than counter ions (H^+) [37], because the ionic

RSC Advances Accepted Manuscript

conductivity is proportional to the square of the charge number of one particle [38]. Consequently, the PSS suspensions including 0.01 mM hydrogen ion can keep the conductance equivalent to 1 mM solution of hydrochloric acid [39]. The suspension is expected to reveal such small values of C_D that $1/C_D > 1/C_H$.

This report is directed to finding the ionic concentrations at which the component of C_D can be extracted from the observed capacitance. The extraction technique is to plot of $1/C$ against $1/\cosh(F\phi/2RT)$, which is expected to show linearity with the intercept of $1/C_H$. Our concern is whether experimental values of the slope, $(2\varepsilon_0\varepsilon_r F^2 c/RT)^{-1/2}$, agree with the theoretical ones or not. The deionized PSS suspensions are used here in order to sustain accuracy of the impedance data against high solution resistance. Reference electrodes such as Ag|AgCl cannot be used here because they increase ionic concentrations by leakage of ions [40]. Therefore we use a two-electrode system composed of two parallel platinum wires [36,39,41-43]. Before applying Eq. (3) to the data of the latex suspensions, we examine the validity of the proportionality of C_D to $\cosh(F\phi/2RT)$ by solving the Poisson-Boltzmann equation for the suspensions.

2. Experimental

2.1. Chemicals

Water used was ion-exchanged at first, distilled and then ion-exchanged again by a ultrapure water system, CPW-100 (Advantec, Tokyo). The purified water exhibited the ionic resistivity of 18 MΩ cm in the water system. The conductivity of the sampled water did not increase at least for 3h if it was sealed against air [40]. Styrene was distilled before the polymerization, according to ref. [36]. Other chemicals were of analytical grade, and were used as received.

RSC Advances Accepted Manuscript

2.2. Synthesis of polystyrenesulfonate latex suspensions

Polystyrenesulfonate latex was synthesized by the method in the previous paper [36]. Purification was carried out three times by the iterative steps of the addition of pure water to the suspension, of centrifugation, and of decantation. The centrifugation was made at 4600 *g* with a refrigerated centrifuge, SRX-201 (Tomy, Tokyo) for 50 min. Sodium ion in the suspension was exchanged into hydrogen ion by adding 1 mol dm^{-3} HCl to the suspension and by being stirred gently for 14 h. In order to remove residual H^+ and Cl^- thoroughly, the purification was repeated more than 5 times until the pH value of supernatant reached 7.

The synthesized particles had uniform diameter, 3.33± 0.05 μm, determined by an optical microscope, VMS-1900 (Scalar, Tokyo), in the wet state. The amount of hydrogen ion on the latex particle was determined by titration with NaOH under monitoring of the conductivity of the suspension [36]. The turning point of the titration curve allowed us to determine the number of the sulfonate moieties per particle, $n = 6.7 \times 10^8$ [39]. Concentration of the PSS suspension was determined by drying a give volume (3 cm^3) of an aliquot of a stock PSS suspension in a vacuum oven, by weighing the dried aliquot, and by dividing the weight by the weight of one particle to yield the number of the particles, where the weight of one particle was evaluated from the product of the volume of one particle by the density (1.05 g cm^{-3})) of PSS.

2.3. Measurements and instrumentation

Electrodes were two platinum wires 0.1 mm in diameter. One wire was fixed in solution with a beam, and the other was mounted on an optical *xy* positioner so that the distance, *d*, between the two wires was adjusted. The immersion length of the wire, *L*, was controlled with a lab jack. Values of *d* and *L* were read through an optical

RSC Advances Accepted Manuscript

microscope. A typical value of L was 4 mm. The cell structure was similar to the illustration previously [36].

The potentiostat was Compactstat (Ivium, Netherlands), equipping a lock-in amplifier. Applied alternating voltage was 10 mV in amplitude. The potentiostat for voltammetry at extremely low scan rates was HECS 972 (Huso, Kawasaki), controlled with a homemade software. Solution was deaerated by nitrogen gas for 15 min before each voltammetric run. Delay of the potentiostat was examined by the same process as in the previous report [41]. Phase sensitivity was estimated by use of a series combination of a film capacitor 0.2 μF and a carbon resistance 1 MΩ. When the ratio of out-of-phase component to in-phase one was less than 0.001, the out-of-phase was observed to be underestimated.

3. Results and Discussion

3.1. Impedance of ionized latex suspensions

We observed through the optical microscope that the latex particles near the platinum electrode in the suspension were oscillating by the Brownian motion. When the electrode was withdrawn from the suspension, no particles were detected on the electrode. Therefore the particles are not adsorbed on the electrode.

The ac impedance of the deionized suspension between the two wire electrodes was obtained at zero dc voltage in the two-electrode system. Figure 1 shows Nyquist plots obtained in hydrochloric acid. All the plots fell on each line, suggesting only the participation in the double layer impedance rather than faradaic impedance. The lines support the validity of the Constant Phase Element [44-47]. The extrapolation of the line to $Z_2 = 0$ for infinite frequency yields the solution resistance, R_s [48]. The method of determining R_s by the two wire electrodes has been demonstrated to be valid [41]. The values of the resistances of HCl were inversely proportional of concentrations of HCl.

RSC Advances Accepted Manuscript

Therefore the evaluation of R_s should be correct. Figure 1 also shows the Nyquist plot for the PSS suspension in which the concentration of free hydrogen ion was 0.01 mM. The value of R_s in the suspension was close to that of 1 mM HCl. Consequently the conductance of the suspension is not brought about by the free hydrogen ion but by the condensed charge of the latex particles [39].

The ac-current, I, in the electric double layer capacitance, C_d, responding to the ac voltage, $V = V_o\exp(i\omega t)$, is given by the time-derivative of the double layer charge, q, i.e., $I = dq/dt$, where i is the imaginary unit, ω is the angular velocity and V_o is the ac-amplitude. When the capacitance is frequency-dependent, the current is expressed by

$$I = \frac{d\left(C_d(\omega)V(t)\right)}{dt} = C_d(\omega)\frac{dV(t)}{dt} + V(t)\frac{\partial C_d(\omega)}{\partial \omega}\frac{d\omega}{dt} \qquad (4)$$

The first term on the right hand side is $i\omega C_d V$, belonging to the out-of-phase. In contrast the second term includes no imaginary number, and hence belongs to the in-phase, i.e. a resistive component. Since the current in Eq. (4) is a sum of the real and the imaginary currents, the equivalent circuit can be represented as a parallel combination of the out-of-phase (defined as C_p) and the resistance ($1/(\partial C_d/\partial t) = R_p$). Then the double layer capacitance, C_d, conventionally used is given by

$$i\omega C_d = 1/R_p + i\omega C_p \qquad (5)$$

The present measurement is made at two identical wire electrodes in the two-electrode system. The total impedance is a series combination of the solution resistance, R_s, and two parallel combinations of C_p and R_p, each representing C_d at one Pt|solution interface, as is shown in Fig. 2. This equivalent circuit allows us to evaluate the frequency-dependent capacitance. The frequency-dependence of R_p ought to vary Z_1 with frequency. Therefore the plots in Fig. 1 are tilted from a vertical line.

We obtain the expressions for the in phase and the out of phase components from the equivalent circuit in Fig. 2, as follows

RSC Advances Accepted Manuscript

$$Z_1 + iZ_2 = R_s + \frac{2}{1/R_p + i\omega C_p}$$

$$Z_1 - R_s = \frac{2R_p}{1+(\omega C_p R_p)^2}, \quad Z_2 = \frac{-2\omega C_p R_p^2}{1+(\omega C_p R_p)^2} \tag{6}$$

The explicit forms of C_p and R_p are given by

$$C_p = \frac{-Z_2}{\omega}\frac{1}{(Z_1 - R_s)^2 + Z_2^2}, \quad R_p = \frac{(Z_1 - R_s)^2 + Z_2^2}{2(Z_1 - R_s)} \tag{7}$$

Values of C_p and R_p were determined from Z_1 and Z_2 at each frequency by use of Eq. (7).

Figure 3 shows logarithmic variations of C_p with logarithm of frequency ($f = 2\pi\omega$) in the PSS suspension and HCl solutions.

Values of C_p show linear relations except for the plot at the low concentration (0.05 mM) of HCl. Low ionic concentrations increase the solution resistance, which degrades accuracy of the impedance data. The linearity suggests

$$C_p = (C_p)_{1Hz} f^k \tag{8}$$

where k is a dimensionless constant and $(C_p)_{1Hz}$ is the capacitance at f = 1 Hz. The linearity is valid for concentrations over 0.1 mM HCl, with the mostly common value k = -0.21. The independence of C_p from ionic concentrations agrees with the previous results [43]. It is ascribed to the observation that a main variable of C_p is a dipole moment of a oriented solvent molecule rather than ions or dielectric constants [43]. C_p itself has a linear relation with log f. Since $\ln(a + x) \approx \ln(a) + x/a$ for small values of x, the linearity of log C_p with log f is equivalent to that of C_p with log f. The linear relation has been demonstrated to hold not only for aqueous solutions including several kinds of salts and their concentrations [41,42] but also various organic solvents [43]. It is also valid at the crystalline surface of graphite, i.e. highly ordered pyrolytic graphite [49].

RSC Advances Accepted Manuscript

The frequency-dispersion is thought to be caused by surface roughness [50-53]. Since crystalline surface always contains a number of defects in order to stabilize entropically the surface energy, the frequency-dispersion is necessarily measured in the capacitance.

We evaluated R_p from values of Z_1 and Z_2 through Eq. (7). Logarithmic values of R_p for 1 mM HCl and PSS are plotted against logarithmic frequency in Fig. 4. They fall on each line, of which slopes are -0.69 and -0.76, respectively. Therefore R_p can be expressed by $k_1 / f^{0.69}$ and $k_2 / f^{0.76}$, respectively. Since $1/R_p = \partial C_p/\partial t = (\partial C_p/\partial f)(\partial f/\partial t)$ according to Eq. (4), the slopes of log C_p vs. log f in Fig. 3 can provide $\partial C_p/\partial f$, which may yield the dependence of R_p on f with the help of $f = \omega/2\pi = 1/2\pi t$. The values of the slopes in Fig. 3 are (a) -0.29 and (d) -0.21, which yield the slopes $\partial R_p/\partial f$ = 0.29 -1 = -0.71 and 0.21-1 = -0.79 for Fig. 4(a) and (d), respectively. They are close to those obtained by the slope in Fig. 3. Therefore, the relation $1/R_p = \partial C_p/\partial t$ is valid numerically. R_p at extremely low frequency, i.e. at DC voltage tends to infinity. Then the equivalent in Fig. 2 is represented by C_p-R_s-C_p in series. Consequently no dc current flows for dc potential in a polarized potential domain.

The frequency-dispersion is not included in the GC theory, but occurs at the electrode surface itself as a subject of C_H. Since it is far from a subject of ionic distribution, we regard it as *a priori* fact here.

3.2. Dependence of capacitance on potential

Although we extracted the out-of-phase component, C_p, from C_d, it contains both C_H and C_D. Our aim is to separate the two by use of dependence on dc-potential, E; C_H being independent of E [42,43], and C_D being dependent on E through Eq. (3). It is under the condition, $C_H > C_D$, that variations of C_p with E can be observed. This may be worked out not only for low concentrations near $\phi = 0$ through Eq. (3) but also for low

RSC Advances Accepted Manuscript

frequency through Eq. (8). First, we examine the concentration dependence of C_p vs E curves. Figure 5 shows potential-variation of C_p at 1.5 Hz in the suspension and HCl with several concentrations. Since the impedance was measured between the two Pt wires in the two-electrode system, the shape should be symmetric with respect to $E = 0$ V. The potential here is not measured from a reference electrode, but is the voltage between the two almost identical electrodes. Its meaning will be discussed in Fig. 8. The values of C_p for HCl were invariant to E at [HCl] > 0.1 mM. A valley shape appeared when the concentration decreased to 0.05 mM. It was not recognized in HCl solution with 0.01 mM because of large noises of C_p. On the other hands, a valley shape clearly appeared in the PSS suspension with acceptable reproducibility (in Fig. 5(d)) although the free concentration of H^+ in the suspension was 0.01 mM. Those less noises are ascribed to the enhanced conductivity with the help of the highly charged latex particles.

The simulation study has pointed out that the ionic contribution of the capacitance should be smaller than that predicted by the GC theory because of hard core exclusion of solvents, ionic correlations and electrostatic repulsion [54]. Application of this concept could allow us to extract the ionic contribution from the observed capacitance more easily than the prediction. Our experimental results, however, suggest the difficulty of the extraction.

The second variable satisfying $C_H > C_D$ is the ac frequency. Figure 6 shows variations of C_p with E at some frequencies in (A) 0.05 mM HCl and (B) the PSS suspension. The C_p values of the HCl solution for $f > 30$ Hz did not vary with the potential, whereas those for $f < 10$ Hz showed a valley shape, as is shown in Fig. 6A. According to Eq. (8), C_p is evaluated to be smaller at higher frequency, and so C_H becomes smaller. Then the measured values of C_d is mainly determined by C_H rather than C_D through Eq. (1). Therefore the potential dependence is extinguished at high frequency."

In contrast, the PSS suspension exhibited valley shapes even for high frequency (f< 10 kHz). Therefore the potential dependence can be obtained accurately by use of the

RSC Advances Accepted Manuscript

deionized PSS suspension. The potential of the bottom of the valley may correspond to point of zero charge (PZC). The PZC here is at 0 V because of the use of the symmetric two-electrode system. No valley was obtained in the three-electrode system because of leakage of ions from a reference electrode [40]. In other words, it is difficult to determine values of the PZC on a reference electrode potential scale. Reported values of the PZC may be at a bottom of valley caused by faradaic processes [42].

The valleys in Fig. 6 might be caused by erroneous data analysis such as in subtraction of R_s near E = 0 V. A technique of detecting the valley without any data analysis is cyclic voltammetry. Cyclic voltammetry was made in the PSS suspension with the extremely low ionic concentration at very low scan rates in the two-electrode system in order to exhibit a valley shape. Usage of a reference electrode increased ionic strength not to exhibit any valley. Figure 7 shows the slow scan voltammogram in the PSS suspension. A valley shape appeared at E = 0 V for iterative scans in both the anodic and the cathodic scan only at the scan rates as slowly as 1 mV s^{-1}. Therefore it should be caused by the capacitance. The appearance of the valley in voltammograms may not have been reported yet, to our knowledge. No valley was observed in HCl solution.

We attempt to separate C_p into C_H- and C_D-components by use of the plots of $1/C_p$ against $1/\cosh(F\phi/2RT)$ with an expectation of exhibiting linearity. We will demonstrate in section 3.4 that C_D for the PSS suspension can be expressed by the same potential dependence as in Eq. (3). It is necessary to make relation between ϕ in the GC-theory with experimentally controllable voltages, E. The predicted distribution of the potential in solution, ϕ_S, is illustrated in Fig. 8, where superscripts, A and C, mean the anode and the cathode, respectively. ϕ_E is the potential of the electrode, ϕ_{S0} is the potential at the electrode on the solution side, and ϕ_{Sx} is the potential at x_2. The voltage, $\phi_E^A - \phi_{S0}^A$, is the same value as $\phi_E^C - \phi_{S0}^C$, because the two electrodes are the common material (Pt).

RSC Advances Accepted Manuscript

Therefore, the applied voltage is ϕ_E^A - ϕ_E^C, which is equal to ϕ_{S0}^A - ϕ_{S0}^C. It can be written in terms of the sum of the three voltages

$$E = \phi_{S0}^A - \phi_{S0}^C = \left(\phi_{S0}^A - \phi_{Sx}^A\right) + \left(\phi_{Sx}^A - \phi_{Sx}^C\right) + \left(\phi_{Sx}^C - \phi_{S0}^C\right) \quad (9)$$

The middle term represents the sum of the *IR*-drop and the voltage by the ion distributions due to the GC-theory between the two electrodes. Since our data of C_p do not contain any *IR*-drop, the middle term equals 2ϕ in the GC-theory. Then Eq. (9) is reduced to

$$E = \left(\phi_{S0}^A - \phi_{Sx}^A\right) + 2\phi + \left(\phi_{Sx}^C - \phi_{S0}^C\right) \quad (10)$$

All the observed capacitance vs. potential curves were approximately symmetric with respect to E = 0 V. The symmetry implies that the ϕ = [E-(ϕ_{S0}^A-ϕ_{Sx}^A)-(ϕ_{S0}^C-ϕ_{Sx}^C)]/2 at the anode should be the same as that at the cathode. We now define the dimensionless unknown variable as

$$r = -\left(\phi_{S0}^A - \phi_{Sx}^A + \phi_{Sx}^C - \phi_{S0}^C\right)/2\phi \quad (11)$$

The meaning of r is the ratio of the voltage in the Helmholtz layer to the externally controlled voltage. Then Eq. (10) is reduced to $E = 2\phi(1 - r)$, and Eq. (3) can be rewritten as

$$C_D = \sqrt{2\varepsilon_r\varepsilon_0 F^2 c / RT}\cosh\left(FE/4(1-r)RT\right) \quad (12)$$

Figure 9 shows the plot of $1/C_p$ against 1/cosh(FE/4(1-r)RT) in the PSS suspension for f = 10 Hz at some values of r. With an increase in r, the fitting curves by a quadratic equation vary from a concave (a) to a convex (c). A line is realized for r = 0.4 ± 0.2, indicating that a quarter of the applied voltage contributes to determination of x_2-potential. The linear variation was found also for 0.05 mM HCl solutions although it contains large errors.

RSC Advances Accepted Manuscript

The linearity in Fig. 9 seems to support the GC theory. However, the slope increased with an increase in the frequency for $f < 10$ Hz, as shown in Fig. 10 for (A) HCl solution and (B) PSS suspension. This is inconsistent with Eq. (12) for the slope. The average values of the slopes of curves (a)-(c) in Fig. 10(A) and 10(B) are 0.63 F^{-1} m^2, and 0.9 F^{-1} m^2, respectively. On the other hands, the calculated values of $(2\varepsilon_0\varepsilon_r F^2 c/RT)^{-1/2}$ are 61 F^{-1} m^2 and 140 F^{-1} m^2, respectively, at c = 0.05 mM and 0.01 mM for ε_r = 78. The experimental values are two orders of the magnitude smaller than the calculated ones. The disagreement indicates that capacitances other than C_D should be involved in parallel to C_D. The GC-capacitance results from an excess amount of accumulated ions by the electric field, but does not include any contribution from solvent molecules. In section 3.5, we will take into account a contribution of solvent molecules by the electric field, like the inner layer capacitance.

The capacitance (Eq. (3)) by the Gouy-Chapman theory has some limitations in finite size of ions and saturation of dielectric constants. We first discuss the effect of finite size by use of the lattice-gas model by Kornyshev [15]. Since the lattice-gas model includes a distribution of ions on the lattice, there is no possibility of overlapping ions. The capacitances with the overlap, C_D, has been given for $C_{D0} = (2\varepsilon_0\varepsilon_r F^2 c/RT)^{1/2}$ by [15]

$$\frac{C_D}{C_{D0}} = \frac{\cosh(F\phi/2RT)}{1+X}\sqrt{\frac{X}{\ln(1+X)}} \qquad (13)$$

where $X = 2\gamma\sinh^2(F\phi/2RT)$ and $\gamma = 2c_{ion}/c_{max}$. Here, c_{ion} is concentration of ion and c_{max} is that of available lattice sites. In other words, γ corresponds to the molar ratio of the anion and the cation to the solvent molecules. Eq. (13) for γ = 1 and 0 represents the capacitance in the completely dissociated electrolyte and in electrolytes with extremely low concentrations, respectively. The latter case is given by $C_D = \cosh(F\phi/2RT)C_{D0}$, which is equivalent to Eq. (3). The U-shape means the potential dependence stronger than the potential-dependence of the GC theory, facilitated by finite size effect. Potential

RSC Advances Accepted Manuscript

variations for several values of γ are plotted in Fig. 11. With a decrease in the concentration ($\gamma \to 0$), the U-shape variation is smoothed. Our experimental data for the 0.05 mM HCl (Fig. 6(A)) were plotted also in Fig. 11 so that the capacitance values were normalized by C_p at E = 0 V. They roughly correspond to Eq. (13) γ = 0.15, whereas 0.05 mM is equivalent to $\gamma = 1.8\times10^{-6}$ (= 2×0.05 mM / 55.5 M). The finite size effect does not interpret the U-shape of our experimental data. This effect is remarkable at high concentrations, whereas U-shapes can be observed experimentally only at extremely low concentrations.

Saturation of dielectric constants decreases C_D through ε_r in Eq. (3). The value of C_{D0} for ε_r = 78 of bulk water and is ε_r = 6 [31] are, respectively, 7.2 and 2.0 μF cm^{-2}at c = 1 mM, calculated from Eq. (3) at ϕ = 0. The dielectric saturation has no effect on the shape of capacitance vs. potential curves.

3.3 Expression for capacitance by ionic distribution in latex suspensions

We derive here the expression for the capacitance by the ionic distribution in latex suspensions on the basis of the Poisson-Boltzmann equation under our experimental conditions. Sulfonic acid moieties in a PSS latex particle are dissociated in the deionized suspension into $-SO_3^-$ and H^+ through the reaction

$$(-SO_3H)_n \leftrightarrow (-SO_3H)_{n-z} + (-SO_3^-)_z + zH^+ \qquad (14)$$

where n is the number of sulfonic moieties per particle, and z is the number of $-SO_3^-$ and H^+. The dissociated H^+ is released into the solution, whereas the dissociated $-SO_3^-$ is immobilized in the latex particle. Since the values of n and z in the present experiment are $n = 6.7\times10^8$ and $z = 6.7\times10^6$, only 1 % of the sulfonic acid moieties are dissociated.

The deionized suspension including N latex particles in a unit volume contains Nz dissociated hydrogen ions. A planar electrode is inserted in the suspension to apply voltage. Let the inner potential in solution at a location x from the electrode be $\phi(x)$. The

RSC Advances Accepted Manuscript

number density of hydrogen ion in equilibrium with the potential in the thermal bath is given by the Boltzmann distribution, $n_+ = Nz\exp(-e\phi/k_BT)$, where e is the elementary charge, and k_B is the Boltzmann constant. If the latex particle were to have the charge $-ze$ in the form of a point charge, the Boltzmann distribution would be expressed by $n_- = N\exp(ze\phi/k_BT)$. The charge $-ze$ is, however, dispersed within the latex sphere 3.3 μm in diameter or 19 μm^3 in volume so that the average concentration is z/19 μm^3 or 0.6 mM. This low concentration makes $z SO_3^-$ ions fluctuated independently in a thermal bath. As a result, the Boltzmann factor is $\exp(e\phi/k_BT)$ rather than $\exp(ze\phi/k_BT)$. The role of the latex is to encompass z anions in the sphere without taking a point charge. Then the number density of the anions is given by $n_- = N\exp(e\phi/k_BT)$. The charge density at x is expressed by

$$\rho = Nze\left[\exp\left(-e\phi/k_BT\right)-(1/z)\exp\left(e\phi/k_BT\right)\right] \qquad (15)$$

The second term in the bracket can be rewritten as $(1/z)\exp(e\phi/k_BT) = \exp[(e\phi - k_BT \ln z)/k_BT]$. This indicates that the electrostatic energy, $e\phi$, is stabilized by the amount of the entropic term, $k_BT\ln z$, owing to the confinement of z sulfonic ions within the particle.

When we introduce the following potential shifted by the entropic term

$$\phi_z = \phi - \left(k_BT/2e\right)\ln z \qquad (16)$$

Eq. (15) is reduced to

$$\rho = N\sqrt{z}e\left[\exp\left(-e\phi_z/k_BT\right)-\exp\left(e\phi_z/k_BT\right)\right] = -2N\sqrt{z}e\sinh\left(e\phi_z/k_BT\right) \qquad (17)$$

Then the Poisson equation is given by

$$\frac{d^2\phi_z}{dx^2} = \frac{2N\sqrt{z}e}{\varepsilon_0\varepsilon_r}\sinh\frac{e\phi_z}{k_BT}$$

Multiplying the terms on the both hand sides by $d\phi_z/dx$, and integrating the resulting equation on the boundary conditions of $\phi_z = 0$, $d\phi_z/dx = 0$ at $x \to \infty$, we have

$$\left(\frac{d\phi_z}{dx}\right)^2 = \frac{8N\sqrt{z}k_BT}{\varepsilon_0\varepsilon_r}\sinh^2\frac{e\phi_z}{2k_BT} \qquad (18)$$

RSC Advances Accepted Manuscript

The left hand side in Eq. (18) is the same as $(\mathrm{d}\phi/\mathrm{d}x)^2$. The surface charge density at the electrode is given by

$$\sigma = \varepsilon_0\varepsilon_\mathrm{r}\left(\frac{\mathrm{d}\phi}{\mathrm{d}x}\right)_{x=0} = \left(8N\sqrt{z}\varepsilon_0\varepsilon_\mathrm{r}k_\mathrm{B}T\right)^{1/2}\sinh\frac{e\phi_0}{2k_\mathrm{B}T} \qquad (19)$$

The capacitance by the ion distribution is expressed by

$$C_\mathrm{Dltx} = \frac{\mathrm{d}\sigma}{\mathrm{d}\phi_0} = e\sqrt{\frac{2N\sqrt{z}\varepsilon_0\varepsilon_\mathrm{r}}{k_\mathrm{B}T}}\cosh\left(\frac{F\phi_0}{2RT}\right) \qquad (20)$$

The potential dependence in Eq. (20) is the same as that (Eq. (3)) by Gouy-Chapman equation. When we express the concentration of the dissociated hydrogen ions as molarity, $c_\mathrm{H,ltx}$, = Nz/N_A, the pre-cosh term in Eq. (20) is $F(2c_\mathrm{H,ltx}\varepsilon_0\varepsilon_\mathrm{r}/zRT)^{1/2}$, where N_A is the Avogadro constant. Only the difference between Eq. (3) and (20) lies in the expression for the concentration. Consequently the capacitance in the suspension at $\phi_0 = 0$ is smaller than that in acid by $z^{-1/2}$.

It is of interest to consider the difference between the length of the ionic atmosphere, λ, of ordinary multi-valence electrolytes and that of the PSS latex. When the potential decay is expressed by the form of $\exp(-\kappa x)$ for a constant κ, the length can be defined as $\kappa^{-1} = \lambda$. We will obtain the exponential form of the solution of the Poisson-Boltzmann equation. The ordinary electrolyte with the z-charged cation and z-charged anion obeys the following Poisson-Boltzmann equation

$$\mathrm{d}^2\phi/\mathrm{d}x^2 = (2zeN/\varepsilon_0\varepsilon_\mathrm{r})\sinh(ze\phi/k_\mathrm{B}T) \qquad (21)$$

When a value of $ze\phi/k_\mathrm{B}T$ is close to zero, the above equation is approximated as

$$\mathrm{d}^2\phi/\mathrm{d}x^2 = \lambda_{z\text{-}z}^{-2}\phi \qquad (22)$$

where

$$\lambda_{z-z} = \sqrt{\varepsilon_0\varepsilon_\mathrm{r}RT/2c}/zF \qquad (23)$$

Since a solution of Eq. (22) is $\exp(-x/\lambda_{z\text{-}z})$, $\lambda_{z\text{-}z}$ is nothing but the length of the ionic atmosphere. The length is inversely proportional to z. On the other hands, the length of the latex suspension can be obtained from the Taylor expansion of the term on the right

RSC Advances Accepted Manuscript

hand side in Eq. (17), which yields $-(2cz^{1/2}F^2/RT)\phi_z$. Then the length for the latex suspension is expressed by

$$\lambda_{\mathrm{ltx}} = \sqrt{\varepsilon_0 \varepsilon_{\mathrm{r}} RT / 2c_{\mathrm{H,ltx}}} / z^{1/4} F \qquad (24)$$

The numerical value of the length by Eq. (24) for $c_{\mathrm{H,ltx}}$= 0.01 mM and $z = 6.7\times10^6$ is 1.9 nm, which is much smaller than the diameter of the PSS particle (3.3 μm). Therefore the ionic atmosphere is formed within the particle. Since $-SO_3^-$ can move in the particle through the reaction $-SO_3H \leftrightarrow -SO_3^- + H^+$ like a free anion, it is reasonable to generate ionic concentration gradient within the particle as a particle approaches the electrode. Figure 12 shows an illustration of (A) the distribution of H^+ and Cl^- and (B) that of H^+ and $-SO_3^-$ in the PSS latex for z = 3 when the number of ions of HCl is the same as that of PSS. The anion $-SO_3^-$ is driven by the electric field in confinement of the sphere of the particle, as shown by the translation of $-SO_3^-$ in the direction of arrows. As a result, an ionic distribution is formed within the particle, and then the ionic length varies from $\lambda_{1\text{-}1}$ to λ_{ltx}. We compare the length in the PSS suspension with that in HCl at a common concentration of H^+. The ratio, $\lambda_{1\text{-}1}/\lambda_{\mathrm{ltx}}$, is $z^{1/4}$ (= 51) for $z = 6.7\times10^6$, indicating that the PSS suspension has stronger ionic intensity than HCl by 51 times. If all the negative charges on the one PSS particle were to be condensed like a point z-electron charge, the ratio $\lambda_{1\text{-}1}/\lambda_{z\text{-}z} = z$, being of the order of 10^6 might correspond to the ionic length of the order of femto m.

3.4 Capacitance in the GC-layer due to solvent

First, we estimate an approximate value of the capacitance due to solvent molecules in the GC-layer where the electric field causes the dipole of solvent molecules to be oriented toward the electric field. If the electric field is applied to the GC-layer uniformly with thickness

RSC Advances Accepted Manuscript

$$\lambda = \sqrt{\varepsilon_0 \varepsilon_r RT / 2cF^2} \quad (25)$$

the capacitance due to solvent per area is represented by $C_{\text{D-slv}} = \varepsilon_0 \varepsilon_r / \lambda$. This is almost the same as C_D at $\phi = 0$. Consequently, the solvent participates in the capacitance in the GC-layer.

We evaluate more accurately $C_{\text{D-slv}}$. Our model is a laminar of solvent monolayer sheets through which the electric field is applied with the ionic distribution of $e^{-x/\lambda}$. The solvent molecule has the dipole moment μ and the length l along the direction of the dipole. Since dipoles are oriented by the electric field which varies with the distance from the electrode, those closer to the electrode are more oriented than those far from the electrode. As a result, the closer to the electrode is a layer, the larger is its capacitance. Let the molecules in the n-th layer from x_2 have the orientation angle, θ_n, from the direction normal to the electrode surface. According to the concept of the inner layer capacitance (Eq. (2)), the capacitance of one molecule in the n-th layer is given by [43]

$$C_n = \varepsilon_0 / l \cos\theta_n \quad (26)$$

where the saturated dielectric constant is represented by $1/\cos\theta_n$. The laminar of the layers implies the parallel combination of the capacitances:

$$1/C_{\text{D-slv}} = \sum_{n=1} 1/C_n \quad (27)$$

A well-known relation between the angle with the electric field is the Debye equation [55], given by

$$\cos\theta = \mathrm{L}\left(\mu(\mathrm{d}\phi/\mathrm{d}x)/k_B T\right) \quad (28)$$

Here, the function L is defined by

$$\mathrm{L}(x) = \coth(x) - 1/x$$

Inserting Eq. (26) and (28) into Eq. (27) yields

RSC Advances Accepted Manuscript

$$1/C_{\text{D-slv}} = \frac{l}{\varepsilon_0}\sum_{n=1}\left|\mathrm{L}\left(\mu(\mathrm{d}\phi/\mathrm{d}x)_n / k_{\mathrm{B}}T\right)\right| \qquad (29)$$

We use Gouy-Chapman's equation for $\mathrm{d}\phi/\mathrm{d}x$ at small values of $e\phi/k_{\mathrm{B}}T$ in the x-coordinate when the anode and the cathode are set at $x = w$ and $-w$, respectively. We assume that the potential distribution is symmetry with respect to $x = 0$. Therefore the boundary conditions in Fig. 8 can be reduced to $\phi(w\text{-}x_2) = \phi_2$ and $\phi(0) = 0$. The solution of the Poisson-Boltzmann equation for small values of $F\phi/RT$ is given by

$$\varepsilon_0\varepsilon_{\mathrm{r}}\left(\mathrm{d}^2\phi/\mathrm{d}x^2\right) = 2F^2c\phi/RT \qquad (30)$$

The boundary value problem for large x has the following approximate equation:

$$\phi = \phi_2 \mathrm{e}^{(x-w+x_2)/\lambda} \qquad (31)$$

Inserting Eq. (31) into Eq. (29) and replacing the summation by an integral yields

$$1/C_{\text{D-slv}} = \frac{1}{\varepsilon_0}\int_0^{w-x_2}\mathrm{L}\left(\frac{\mu\phi_2}{\lambda k_{\mathrm{B}}T}e^{(x-w+x_2)/\lambda}\right)\mathrm{d}x \qquad (32)$$

Substitution of $(\mu\phi_2/\lambda k_{\mathrm{B}}T)\exp[(x\text{-}w\text{+}x_2)/\lambda] = z$ reduces Eq. (32) to

$$1/C_{\text{D-slv}} = \frac{\lambda}{\varepsilon_0}\int_0^{\mu\phi_2/\lambda k_BT}\{L(z)/z\}\mathrm{d}z \qquad (33)$$

where $(\lambda\phi_2/\lambda k_{\mathrm{B}}T)\exp[(-w\text{+}x_2)/\lambda]$ was regarded as zero. Since z is less than 0.1, the function $\mathrm{L}(z)$ can be approximated to $z/3$. Then the integral is carried out and Eq. (33) becomes

$$C_{\text{D-slv}} = 3\varepsilon_0 k_{\mathrm{B}}T/\mu\phi_2 = 6\varepsilon_0 k_{\mathrm{B}}T/\mu\left(\phi_{\mathrm{Sx}}^{\mathrm{A}} - \phi_{\mathrm{Sx}}^{\mathrm{C}}\right) \qquad (34)$$

This capacitance does not vary directly with the ionic concentration but vary through ϕ_2 which depends on the ionic concentration.

A typical value of $C_{\text{D-slv}}$ in water (μ = 1.84 Debye) is 18 μF cm^{-2} at ϕ_2 = 0.1 V. It is larger than the value for the GC-theory by 30 times. Since the density of ions is much smaller than that of solvent, the capacitance caused by ions ought to be much smaller

RSC Advances Accepted Manuscript

than that by the orientation of solvent dipoles. Therefore it is necessary to take into account the contribution of the orientation of the dipole in the capacitance of the diffuse layer, in addition to the Gouy-Chapman's term,

$$C_{\text{D-ion}} = \sqrt{2\varepsilon_r \varepsilon_0 F^2 c / RT} \qquad (35)$$

Since the orientation is brought about by the electric field which is relaxed with the ionic distribution, it is associated with cosh(*EF*/4(1-*r*)*RT*). Then, the capacitance of the diffuse layer is represented as

$$C_{\text{D}} = \left(C_{\text{D-ion}} + C_{\text{D-slv}}\right)\cosh\left(FE/4(1-r)RT\right) \qquad (36)$$

The measured capacitance is mainly controlled by $C_{\text{D-slv}}$ rather than $C_{\text{D-ion}}$. This prediction is seen in the dependence of the slopes of $1/C_{\text{p}}$ vs. 1/cosh[*FE*(1-*r*)/*RT*] on frequency through Fig. 10, like the frequency-dependence of the inner layer capacitances in Fig. 3.

Eq. (36) implies a parallel combination of $C_{\text{D-ion}}$ and $C_{\text{D-slv}}$, which is in series with C_{H}, as shown in Fig. 13(A). Since $C_{\text{D-slv}}$ depends on the frequency as the inner capacitance does, the measurement of $C_{\text{D-slv}}$ is necessarily associated with the apparent capacitance, $R_{\text{pD-slv}}$, in the form of the inverse proportionality of the frequency, as for the apparent resistance, R_{pH}, in the inner layer. Consequently, the equivalent circuit including the frequency-dependence takes a complicated form as shown in Fig. 13(B). Values of R_{pH} and $R_{\text{pD-slv}}$ at low frequency are large enough to be negligible. Then the circuit in Fig. 13(B) tends to that in Fig. 13(A).

It would be interesting to extract $C_{\text{D,slv}}$ or $C_{\text{D,ion}}$ from C_{p}. A controllable variable of the extraction is the ionic concentration included in Eq. (35). Usage of lower concentrations of PSS suspensions might allow us to evaluate $C_{\text{D,ion}}$, which could be realized by the latex particles with larger values of the sulfonic moiety ($n > 6.7\times10^8$) per particle . Unfortunately, our synthetic technique is not enough at present. Therefore, it is quite difficult to extract the component of GC capacitance from experimentally obtained capacitance.

4. Conclusion

RSC Advances Accepted Manuscript

The answer to the titled question is that it is the capacitance caused by dipole moments of solvent molecules in the diffuse layer rather than the capacitance caused by displacement of ionic charges. It is based on the fact that the observed potential-dependent term is much larger than that by the GC-theory. Since the capacitance by the dipole moments is controlled by the electric field, it contains the potential-dependence in the form of the hyperbolic cosine function. The present discussion is restricted to the system of normal ions in solutions or ionic latex suspensions. It is dangerous to apply directly the present result to ionic liquids.

It is not easy to extract the potential-dependent from the observed double layer capacitance, because values of $1/C_D$ are smaller than those of $1/C_H$. The condition of $1/C_D > 1/C_H$ can be attained by decreasing ionic concentrations less than 0.05 mM. This concentration domain is incompatible with accurate impedance measurements in the context of high solution resistance. The difficulty can be solved by use of deionized latex suspensions, which can support conductivity with low free ionic concentration.

The valley shape appears in cyclic voltammograms in the PSS suspension at very slow scan rates. This is an evidence of the valley shape in capacitive currents. The bottoms of valley in both the capacitance-potential curves and the voltammograms correspond to a PZC. Any reference electrode cannot be used for detection of a valley because a reference electrode increases ionic concentration. Therefore it is difficult to determine s PZC value vs. NHE.

Acknowledgment

This work was financially supported by Grants-in-Aid for Scientific Research (Grant 25420920) from the Ministry of Education in Japan.

References

RSC Advances Accepted Manuscript

[1] R. Hunter, Foundations of Colloid Science, 2nd ed. Oxford University Press: New York, 2001.

[2] V. Bagotsky, Fundamentals of Electrochemistry, 2nd ed., John Wiley & Sons: New York, 2006.

[3] O. Stern, Z. Elektrochem. (1924) 30 508.

[4] N.F. Mott, R.J. Watts-Tobin, Electrochim. Acta 4 (1957) 79.

[5] J.R. Macdonald, C.A. Barlow, J. Chem. Phys. 36 (1962) 3062.

[6] S. Levine, G. M. Bell, A.L. Smith, J. Phys. Chem. 73 (1969) 3534.

[7] J. O'M. Bockris, M.A.V. Devanathan, K. Muller, Proc. R. Soc. London, Ser. A 274 (1963) 55.

[8] B. Damaskin, A.N. Frumkin, Electrochim. Acta, 19 (1974) 173.

[9] R. Parsons, J. Electroanal. Chem. 59 (1975) 229.

[10] R. Parsons, Electrochim. Acta 21 (1976) 681.

[11] G. Gouy, J. Physique 9 (1910) 457.

[12] D.L. Chapman, Phil. Mag. 25 (1913) 475.

[13] C. Outhwaite, L. Bhuiyan, J. Chem. Soc., Faraday Trans. 2, 79 (1983) 707–718.

[14] V. Vlachy, Annu. Rev. Phys. Chem. 50 (1999) 145–165.

[15] A. Kornyshev, J. Phys. Chem. B 111 (2007) 5545–5557.

[16] J. Bikerman, Philos. Mag. 33 (1942) 384–397.

[17] I. Borukhov, D. Andelman, H. Orland, Phys. Rev. Lett. 79 (1997) 435–438.

[18] K. Aoki, Electrochim. Acta 67 (2012) 216.

[19] B. Conway, J.M. Bockris, I. Ammar, Trans. Faraday Soc. 47 (1951) 756-766.

[20] J.R. Macdonald, J. Chem. Phys. 22 (1954) 1857-1866.

[21] J.R. MacDonald, J. Electroanal. Chem. 223 (1987) 1-23.

[22] K. Laidler, J. M.-Gould, Trans. Faraday Soc. 63 (1967) 953-957.

[23] S. Levine, C.W. Outhwaite, L.B. Bhulyan, J. Electroanal.Chem. 123 (1981) 105.

[24] S.L. Carnie, D.Y.C. Chan , D.J. Mitchel, B.W. Ninham, J. Chem. Phys. 74 (1981) 1472.

[25] G.M. Torrie, J.P. Valleau, J. Chem. Phys. 73 (1980) 5807.

[26] W.R. Fawcett, Electrochim. Acta 54 (2009) 4997.

RSC Advances Accepted Manuscript

[27] E.J.F. Dickinson, R.G. Compton, J. Electroanal. Chem. 655 (2011) 23‑31.

[28] E. Dickinson, R. Compton, J. Phys. Chem. C 113 (2009) 17585–17589.

[29] H. Wang, L. Pilon, J. Phys. Chem. C, 115 (2011) 16711–16719.

[30] J. Huang, R. Qiao, B. Sumpter, V. Meunier, J. Mater. Res. 25 (2010) 1469–1475.

[31] R. Rampolla, R. Miller, C. Smyth. J. Chem. Phys. 30 (1959) 566.

[32] J. M. Roberts, P. Linse, J. G. Osteryoung, Langmuir, 14 (1998) 204.

[33] K. Aoki, J. M. Roberts, J. G. Osteryoung, Langmuir, 14 (1998) 4445.

[34] K. Aoki, T. Lei, Electrochem. Commun. 1 (1999) 101.

[35] K. Aoki, C. Wang, Langmuir, 17 (2001) 7371.

[36] K. J. Aoki, X. Zhao, J. Chen and T. Nishiumi, J. Electroanal. Chem. 697 (2013) 5.

[37] K.S. Schmitz, "Macroions on Solution and Colloidal Suspensions", VCH Publishers Inc. New York, 1993, pp. 164-166.

[38] P.W. Atkins, *Physical Chemistry*, Sixth Edition, Oxford University Press, p. 740-750.

[39] X. Zhao, K. J. Aoki, J. Chen and T. Nishiumi, Int. J. Electrochem. Sci. 9 (2014) 2649-2661.

[40] C. Zhang, K.J. Aoki, J. Chen, T. Nishiumi, J. Electroanal. Chem. 708 (2013) 101-107.

[41] K. Aoki, Y. Hou, J. Chen, T. Nishiumi, J. Electroanal. Chem. 689 (2013) 124-129.

[42] Y. Hou, K.J. Aoki, J. Chen, T. Nishiumi, Univ. J. Chem. 1 (2013) 162-169.

[43] Y.Hou, K.J. Aoki, J. Chen, T. Nishiumi, J. Phys. Chem. C 118 (2014) 10153-10158.

[44] G.J. Brug, A.L.G. Eeden, M. S.-Rehbach, J.H. Sluyters, J. Elecroanal. Chem. 176 (1984**)** 275-295.

[45] L. Nyikos, T. Pajkossy, Electrochim. Acta, 30 (1985**)** 1533-1540.

[46] J. Bisquert, G. G.-Belmonte, P. Bueno, E. Longo, L. Bulhoes, J. Electroanal. Chem. 452 (1998) 229-234.

[47] P. Zoltowski, J. Electroanal. Chem. 443 (1998) 149-154.

[48] A.J. Bard, L.R. Faulkner, Electrochemical Methods: Fundamentals and Applications, John Wiley & Sons, 2001, pp. 384-387.

RSC Advances Accepted Manuscript

[49] K.J. Aoki, H. Wang, J. Chen, T. Nishiumi, Electrochim. Acta 130 (2014) 381–386.

[50] J. Bisquert, G. Garcia-Belmonte, P. Bueno, E. Longo, L. Bulhoes, J. Electroanal. Chem. 452 (1998) 229-234.

[51] T. Pajkossy, Solid State Ionics, 176 (2005) 1997-2003.

[52] R. Leek, N.A. Hampson, Surface Tech. 7 (1978) 151-155.

[53] S. Cotgreave, N. Hampson, P. Morgan, M. Welsh, R. Leek, Surface Tech. 13 (1981) 107-110.

[54] S. Lamperski, D. Henderson, Mol. Simul. 37 (2011) 264-268.

[55] P. Debye, Marx' Handbuch der Radiologie; Akademische Verlagsgesellschaft: Leipzig, 6 (1925) 618-680.

RSC Advances Accepted Manuscript

Figure Captions

Figure 1. Nyquist plots of (a) 1 mM, (b) 0.2 mM, (c) 0.05 mM HCl and (d) PSS suspension which contains 0.01 mM free hydrogen ion. The applied ac-voltage had 10 mV amplitude and frequency domain from 10 Hz to 10 kHz.

Figure 2. Equivalent circuit of the series combination of the double layer impedance and the solution resistance R_s. The double layer impedance is composed of a parallel combination of the capacitance, C_p, and the resistance, R_p, both being frequency-dependent.

Figure 3. Variation of C_p in (a) 1 mM HCl, (c) 0.05 mM HCl and (d) PSS suspension (including 0.01 mM H^+) with logarithmic frequency.

Figure 4. Logarithmic variations of R_p in (a) 1 mM HCl and (d) PSS suspension with logarithmic frequency.

Figure 5. Variations of $(C_p)_{1.5Hz}$ with the dc-potential obtained in (a) 1 mM HCl, (b) 0.2 mM HCl, (c) 0.05 HCl and (d) PSS suspension.

Figure 6. Dependence of C_p on the dc-potential in (A) HCl 0.05mM and (B) PSS suspension at f = (a) 1.6, (b) 3.2, (c) 10, (d)100 and (e) 3120 Hz.

Figure 7. Voltammetry in the PSS suspension at the scan rate 1 mV s^{-1}. The scan started at E = 0 V in the positive direction.

Figure 8. Illustration of predicted potential distributions in solution phase and the interfaces. "O", "x" and "w" mean the origin, the coordinate axis, and a half of the distance between the electrodes, used in the next section.

Figure 9. Variations of C_p^{-1} with $\cosh(FE/4(1-r)RT)$ of the PSS suspension at f = 10 Hz for r = (a) 0.0, (b) 0.3 and (c) 0.6.

Figure 10. Plots of the inverse of the capacitance against the inverse of the hyperbolic cosine in (A) 0.05 mM HCl solution and (B) PSS suspension for r = 0.3 at f = (a) 1.5, (b) 5.1, (c) 10 and (d) 100 Hz.

RSC Advances Accepted Manuscript

Figure 11. Variations of Eq. (13) for γ= (a) 0.0, (b) 0.01, (c) 0.1 and (d) 0.2. Circles are the data in Fig. 6(a).

Figure 12. Illustration of ion distribution of (A) HCl and (B) PSS latex for z = 3 with a common concentration of H^+. The left double layer is drawn in contact with the right double layer. The arrows indicate translation of $-SO_3^-$ when Cl^- is replaced by PSS particle.

Figure 13. Equivalent circuit of double layer capacitance, composed of the inner layer capacitance and the two components of diffuse layer capacitance (A) without and (B) with considering frequency-dependence.

RSC Advances Accepted Manuscript

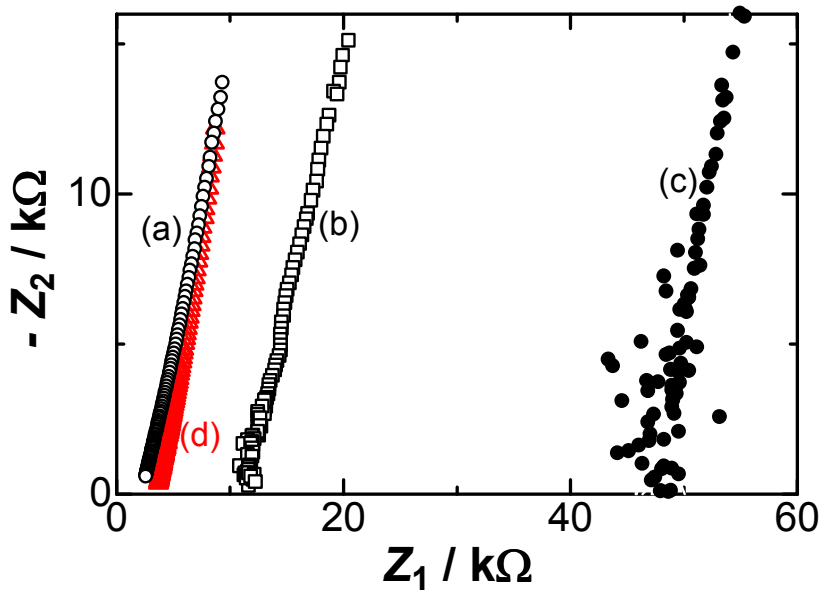

Fig. 1

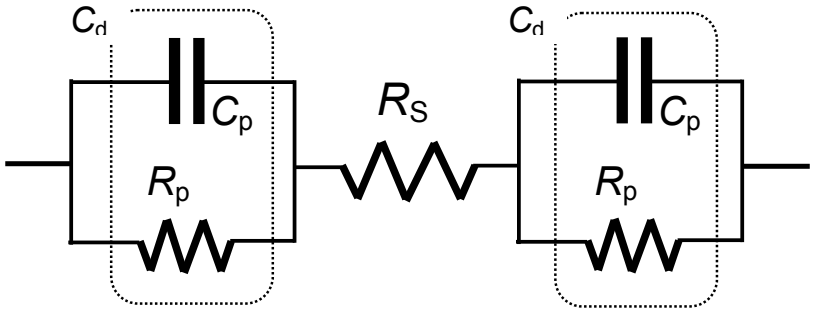

Fig. 2

RSC Advances Accepted Manuscript

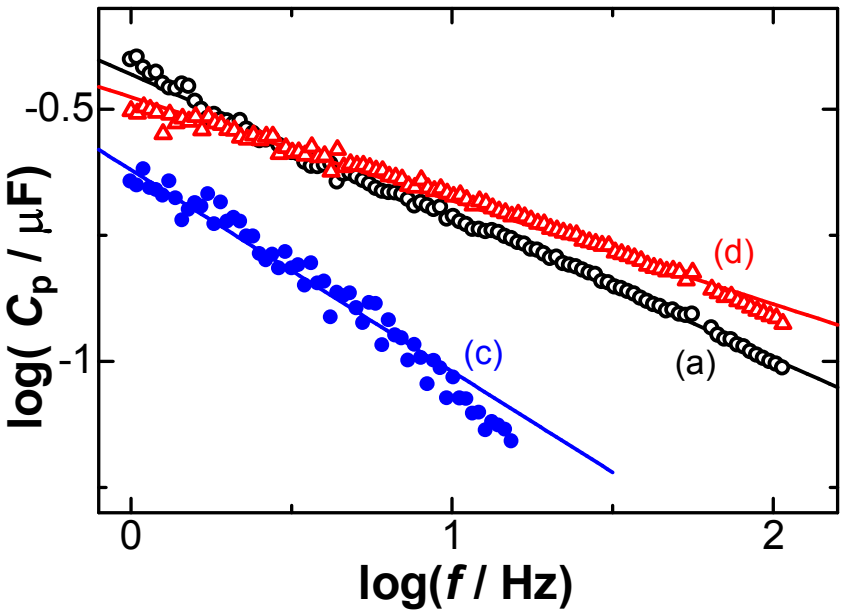

Fig. 3

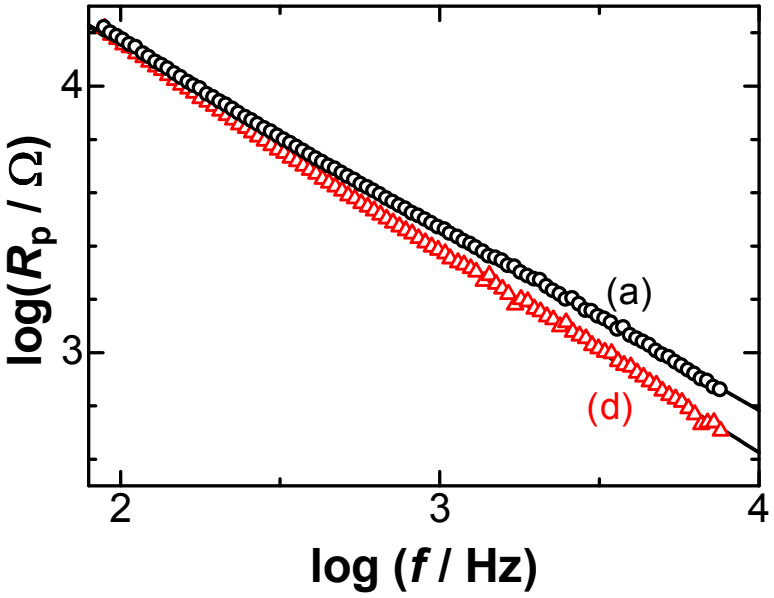

Fig. 4

RSC Advances Accepted Manuscript

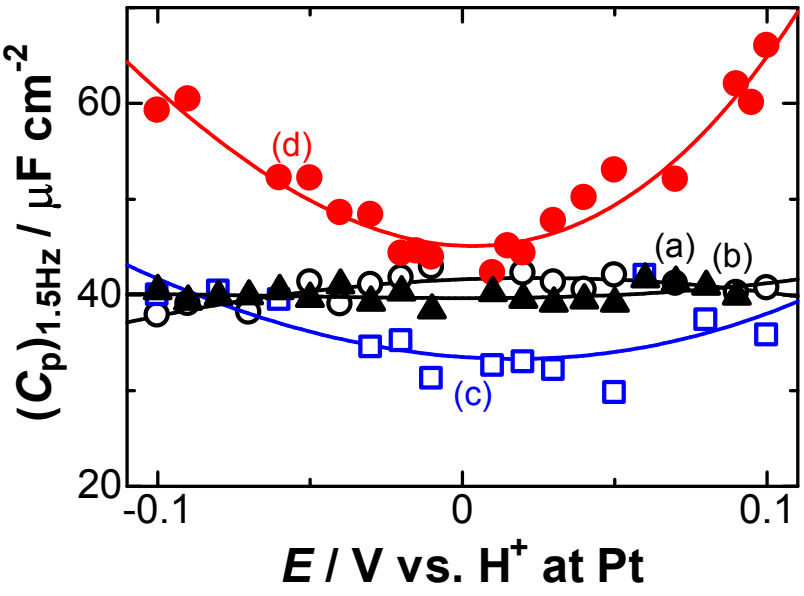

Fig. 5

RSC Advances Accepted Manuscript

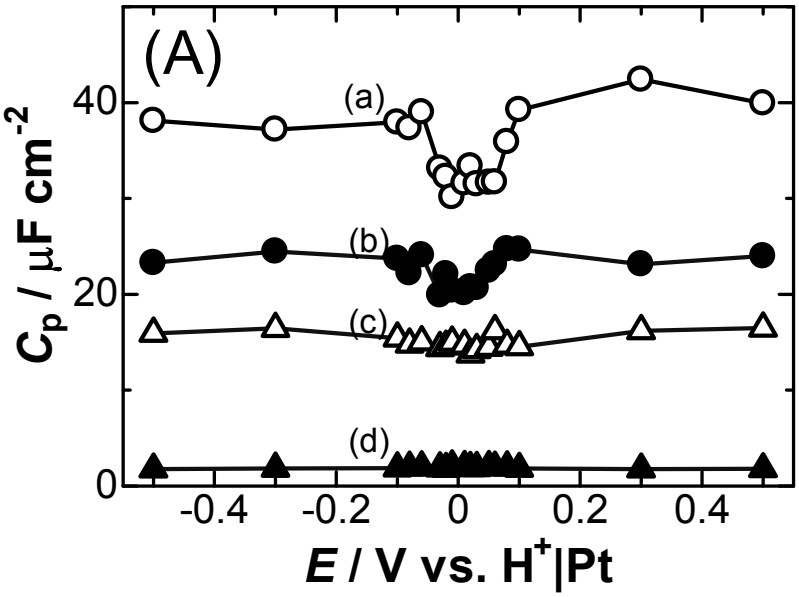

Fig. 6(A)

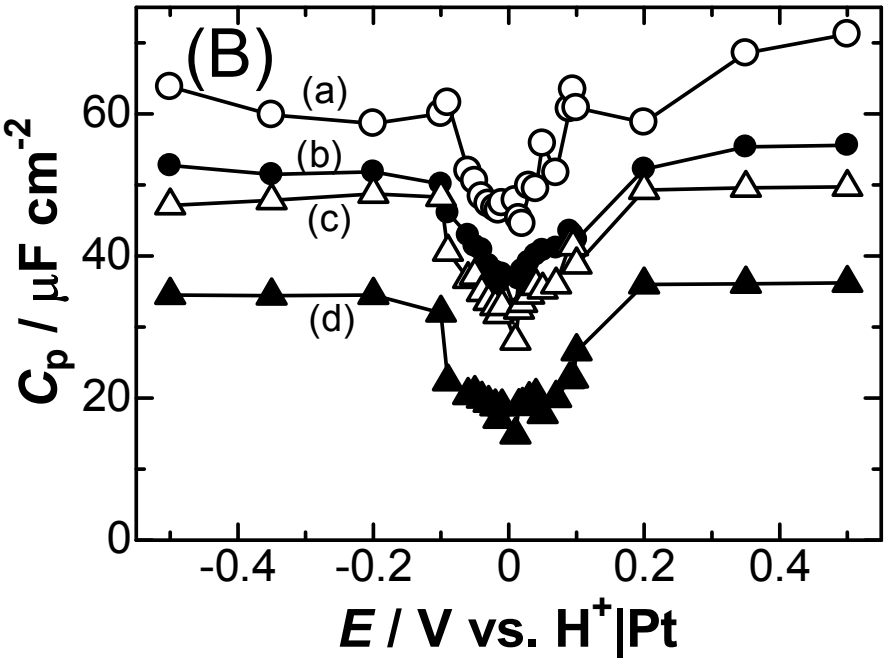

Fig. 6(B)

RSC Advances Accepted Manuscript

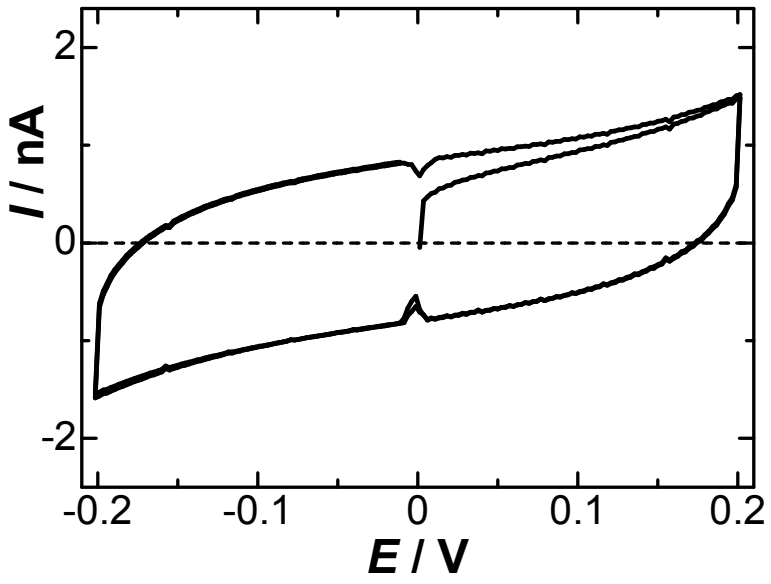

Fig. 7

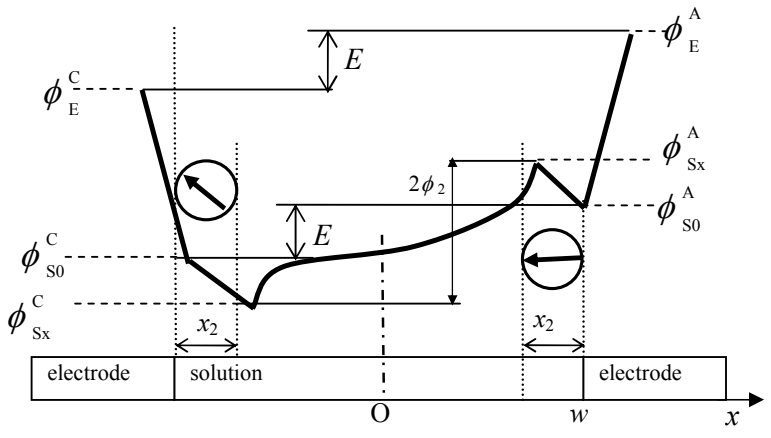

Fig. 8

RSC Advances Accepted Manuscript

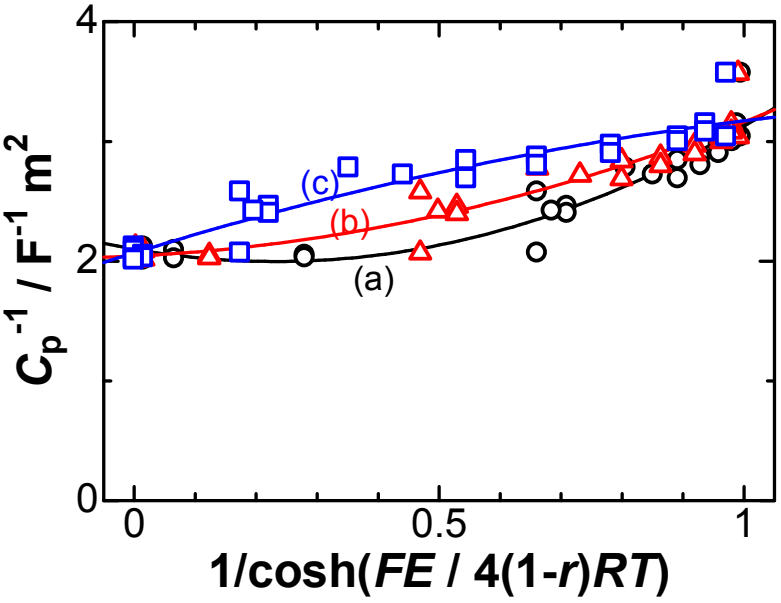

Fig. 9

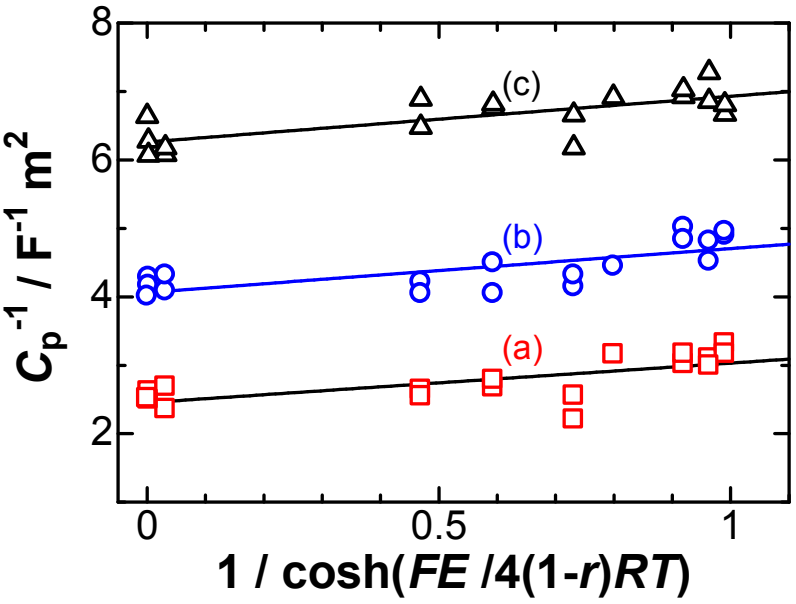

Fig. 10(A)

RSC Advances Accepted Manuscript

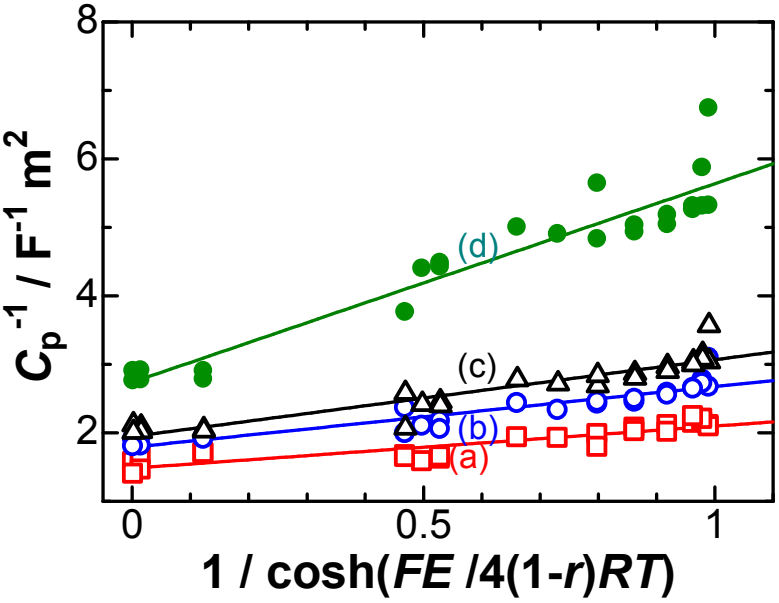

Fig. 10(B)

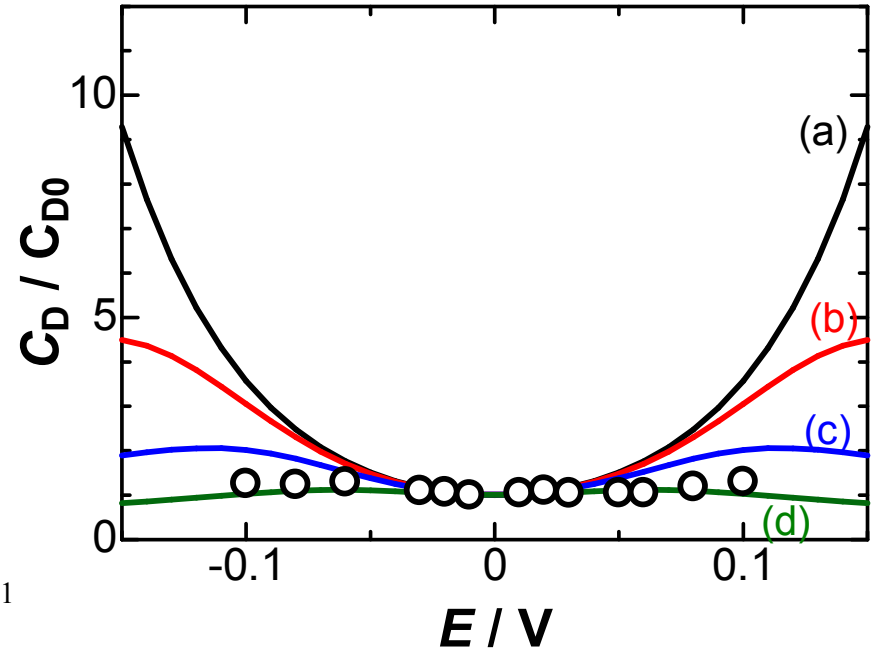

Fig. 11

RSC Advances Accepted Manuscript

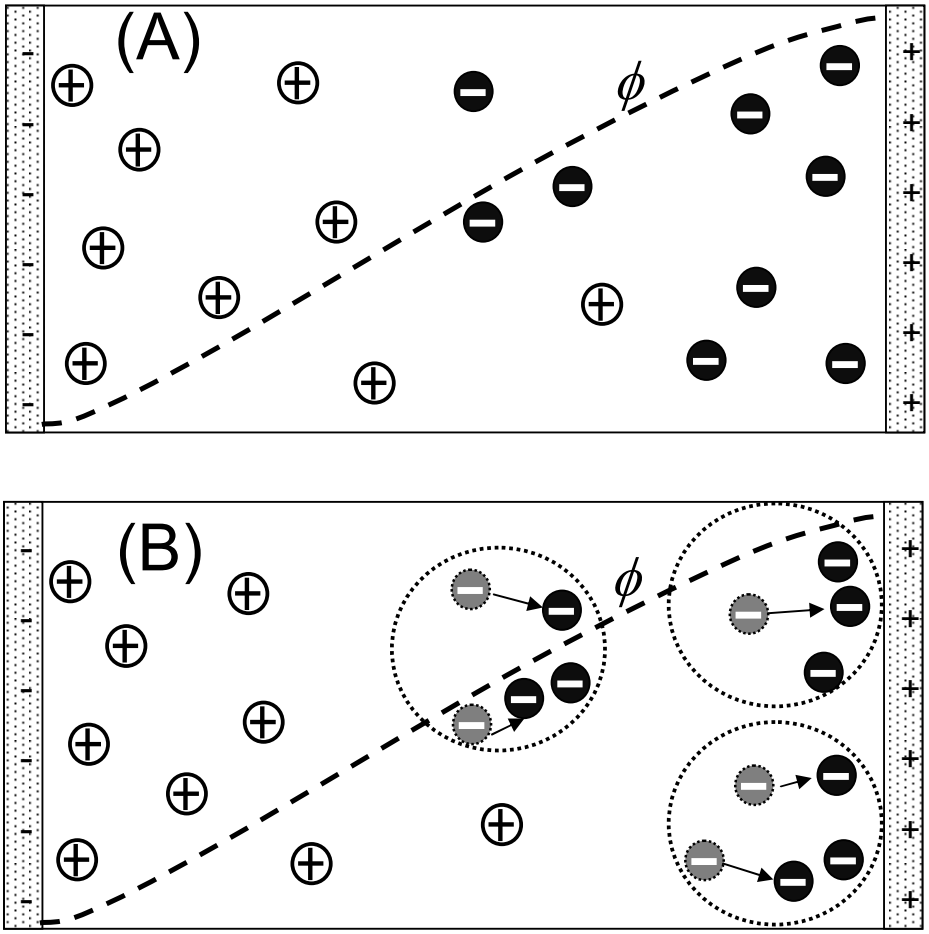

Fig. 12

RSC Advances Accepted Manuscript

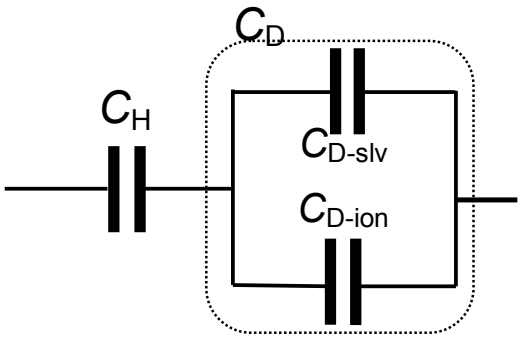

Fig. 13(A)

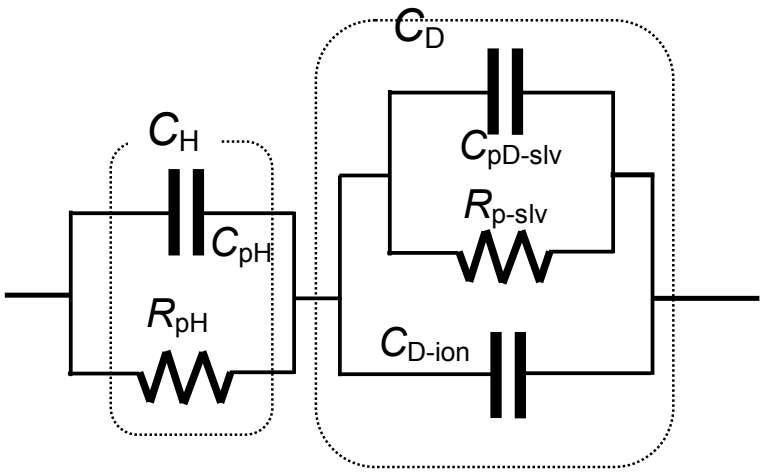

Fig. 13(B)

RSC Advances Accepted Manuscript